International Journal of Biological Macromolecules xxx (2017) xxx–xxx

Contents lists available at ScienceDirect

International Journal of Biological Macromolecules

journal homepage: www.elsevier.com/locate/ijbiomac

Determining mushroom tyrosinase inhibition by imidazolium ionic liquids: A spectroscopic and molecular docking study

Mark P. Heitz*, Jason W. Rupp

Department of Chemistry and Biochemistry, The College at Brockport, SUNY, 228, Smith Hall 350 New Campus Drive, Brockport, NY, 14420, United States

ARTICLE INFO

Article history:
Received 21 August 2017
Received in revised form
30 September 2017
Accepted 11 October 2017
Available online xxx

Keywords:
Imidazolium ionic liquid
Tyrosinase inhibition
Molecular docking

ABSTRACT

The inhibition effects of imidazolium ionic liquids (ILs) on the enzyme kinetics of mushroom tyrosinase is reported. A simple UV-VIS spectrophotometric assay was used to measure the reaction kinetics of the reaction between mushroom tyrosinase and L-dopa. Seven different imidazolium ILs, comprised of 1-alkyl-3-methylimidazolium ($[Im_{n1}^+]$, n = 2, 4, 6) cations paired with several anions that included Cl^-, $[NO_3^-]$, methanesulfonate ($[MeSO_3^-]$), trifluoromethanesulfonate (or triflate, $[TFMS^-]$), and bis(trifluoromethylsulfonyl)imide ($[Tf_2N^-]$). Lineweaver-Burk plots were generated from the recovered k_{cat} and K_m parameters using four to six substrate concentrations per measurement. The results show that mushroom tyrosinase activity was consistently inhibited by all of the ILs and that the type of inhibition was non-competitive in nearly all cases. Only the data for $[Im_{21}^+][Tf_2N^-]$ suggested that the inhibition mechanism was competitive with the substrate. Molecular docking simulations were performed using AutoDock4.2 and AutoDock Vina and revealed that all cations docked in the L-dopa active site. Anions showed varied results that included locations both within and outside of the active site.

1. Introduction

The enzyme tyrosinase, found in melanocytes, plays an important role in the biosynthesis of melanins and other polyphenolic compounds [1]. Melanocytes are cells found in the basal layer of the epidermis and are key in the production of melanin, the pigmentation molecule responsible for skin color and protection of skin cells and DNA from UV damage [2]. Melanin is synthesized by tyrosinase and its formation is rate-limited by the enzymatic reaction. Even when melanocytes become cancerous the melanoma can still produce melanin and it is of interest to note that the elevated expression of the tyrosinase is found in melanoma cells [3] and that the control of *in vivo* melanin production is regulated by the inhibition of tyrosinase activity [4–7]. Previous research highlights that a strategy of targeting tyrosinase with inhibitors can be used to treat melanogenic disorders [4,5,7]. Thus, understanding enzyme-inhibitor interactions effects and how tyrosinase activity is influenced can have a significant impact on the diagnosis and treatment of melanin related diseases. Another important application of tyrosinase chemistry is that it plays a key role in the browning of fruit skin. As a result, the agricultural and food industries are continually seeking ways to reduce the impact of food waste and are interested in identifying tyrosinase inhibitors as a way to prevent over riping of fruit [8,9]. The clear advantage of governing tyrosinase chemistry in this application is increased product shelf life with the potential to effectively increase agricultural yields while simultaneously reducing the economic impact of waste.

Tyrosinase is known to catalyze the hydroxylation of phenolic substrates to catechol derivatives, which in turn are able to further oxidize into orthoquinone products [6,7,10,11]. Biochemical reactions that take place under physiological conditions often rely on catalysts for efficient reactivity and thus enzymatic function can have a significant impact on organisms at the cellular level. Enzymes, like all other catalysts, are characterized by three fundamental properties: 1) increase reaction rates without altering the position of chemical equilibrium; 2) are not consumed and are not permanently altered by the reaction; and 3) acceleration of reaction rates by altering substrate conformation so that the conformation becomes configured to form the transition state intermediate. Catalytic activity involves enzyme/substrate binding to form an enzyme-substrate complex (ES*) in a lock and key manner. Initially, the substrate is bound through noncovalent interactions. It is often the case that both enzyme and substrate are modified by an induced fit process that causes the substrate stresses to further enhance the conversion into the ES* transition state, which results from a weakening of bonds. The ES* state is stabilized by tight enzyme binding that lowers activation energy [10]. Substrates bind to the enzyme active site with specificity and when bound convert into products

* Corresponding author.
E-mail address: mheitz@brockport.edu (M.P. Heitz).

https://doi.org/10.1016/j.ijbiomac.2017.10.066
0141-8130/

that are subsequently released from the enzyme. Active sites can be envisioned as grooves or clefts on the surface of the enzyme that are composed of amino acids from different parts of the polypeptide chains. The specificity of active site interactions are unique to each enzyme and are driven by the specific interactions between the amino acids and substrate. Structurally, the tyrosinase active site has been shown to consist of two Cu^{2+} ions coordinated to two sets of three histidine residues [9]. The crystal structure has been reported and the ribbon structure of tyrosinase with L-dopa incorporated in the active site has been published and made available through the RCSB protein data bank (PDB), structure 4P6S [12]. According to this structure, there are two binding pockes for L-dopa in each of the two chains reported. The binding pockets appear on the enzyme's outer surface and in both cases (for both chains) involve (at least) HIS13, HIS60, HIS204, HIS208, ARG209 residues in addition several other residues that are in positions of close contact (~4 Å).

Ionic liquids (ILs) are often touted as environmentally friendly solvents that are capable of solubilizing a wide variety of poorly water-soluble substrates. ILs, particularly imidazolium derived ILs, have become broadly applied in many industrial applications [13–19] and in agricultural applications such as pesticides and plant growth regulation [20,21]. For example, ternary imidazolium IL systems were studied for use as pretreatment media to reduce biomass recalcitrance and to assess their ability to enhance the efficiency of enzymatic saccharification for biofuel production [19]. Imidazolium ILs also have been used in the synthesis of new ILs based on dicambra (a systemic herbicide) that were designed as alternatives to using free dicambra [21]. Results from this work showed that the ILs had improved properties of increased thermal stability, reduced volatility, and improved efficacy compared to free dicambra. The use of the imidazolium cation was selected for its reported antimicrobial effects against gram-positive and gram-negative bacteria, yeasts, molds, and fungi [21]. The antimicrobial effects of imidazolium ILs have also been studied using human serum albumin (HSA) and demonstrated to have significant antibacterial and antifungal activities [22]. In addition, ILs have been cited as potentially useful for biocatalytic reactions [23–26]. The enzyme kinetics of yeast alcohol dehydrogenase was studied fifteen IL cation/anion pairs, including eight imidazolium ILs and it was reported that anion effects dominated the salt effects on this enzyme [27]. These works, and many others, highlight one of the attractive features of ILs and that is the physicochemical properties can be fine-tuned simply by selecting different combinations of anions and cations. Moreover, attaching various substituents to either the cation or anion makes ILs easy targets for use in task-specific chemical applications. However, as is often the case, chemical applications can signifcantly outpace a systematic, thorough fundamental study of novel chemical systems and ILs are no exception. The inherent problem becomes that broader impacts are not well understood *before* process modification and implementation. For example, while ILs are used to design "greener" chemical processes because of their low volatility, the actual environmental impact is not well defined nor understood. However, this area of focus has been receving increased attention [19–21,28–31]. Since many ILs exhibit significant water solubility, their presence in aqueous waste streams and use in agriculture are clearly direct pathways into the environment. Given the reported biodegradation variability of ILs and therefore the persistance of ILs in water sources and soils, it is important to study the details of molecular interactions between biomolecules and ILs [28–31]. One recent review article has discussed the topic of ILs as they relate to biological activity and highlighted the wide range of effects of several IL classes in the context of medicinal and pharmaceutical applications [32].

When incorporated into an enzyme, ILs have been reported to have mixed effects on activity. In some cases ILs can enhance enzymatic activity and selectivity as highlighted in a recent mini-review by Goldfeder and Fishman [33]. In contrast, the IL cations and anion can disrupt the amino acid interactions and alter the enzyme conformation through alteration of the hydrophobic effect (which governs secondary and tertiary protein structure), hydrophobic hydration, surface tension, and water–water interactions among other factors, all of which induce a corresponding diminution of enzymatic activity [34]. Typically, these structural changes cause disruption to the enzyme's active site and performance can be compromised [35]. A large number of reports have demonstrated that the activity effects in many IL systems can be predicted by the Hofmeister series, where the relative kosmotropicity (order-making or structure-making) or chaotropicity (disorder-making) of the IL ions dictate the outcome of enzymatic activity, particularly in bulk aqueous solutions where the IL ions tend to be solvent separated [36,37]. These general effects have been discussed at length in several reviews [33–35,37–41].

In this work, we report on the reaction kinetics between mushroom tyrosinase and L-dopa measured in the presence of the seven imidazolium-based ionic liquids, shown in Fig. 1. These imidazolium ILs were selected because of their favorable miscibility with aqueous solutions. Moreover, given that imidazolium ILs are by far the most widely studied and applied ILs, their extensive use suggests that they would be the most likely candidates to appear in the environment, whether through aqueous waste streams or direct applications in agriculture [29,31]. We studied the effect of IL cation hydrophobicity by increasing the alkyl chain substituent to determine its impact on enzymatic activity. To elucidate the effect of anion, we selected the $[Im_{21}^+]$ cation to use with several anions anticipating that $[Im_{21}^+]$ would have simultaneously the highest solubility and the weakest direct impact on the enzyme hydrophobic interactions. In the presence of $[Im_{21}^+]$ the anion effect on the resulting enzyme stability and activity should be most clearly delineated. Since anions are reported to have the greater impact on activity and stability [27,35], we were particularly interested to determine the influence of specific ion effects on the tyrosinase activity.

2. Materials and methods

2.1. Materials

Table 1 summarizes each of the ionic liquid abbreviations, complete chemical names along with chemical abstract registry numbers, and purity and sources of chemicals used in this work. All enzyme and substrate solutions were prepared in 50 mM ionic strength and pH = 6.8 potassium phosphate buffer. A concentration of approximately 50 nM tyrosinase was constant across all experiments reported. For convenience, we prepared a stock tyrosinase solution in phosphate buffer such that we could easily micropipette desired volumes for kinetic runs. In the same way, stock L-dopa solutions were always prepared at 1.5 $mg{\cdot}mL^{-1}$. For a kinetic series at a constant [IL], L-dopa concentrations were typically varied between 0.5–3.8 mM by pipetting 200–1500 μL of stock the L-dopa solution. Stock enzyme and substrate solutions were always protected from light, both during experiments and when stored. Storage of all stock solutions was at 4 °C when not in use.

2.2. Methods

2.2.1. Kinetic measurements

To prepare for a series of experiments, solutions were freshly made the afternoon prior to use and then equilibrated overnight at

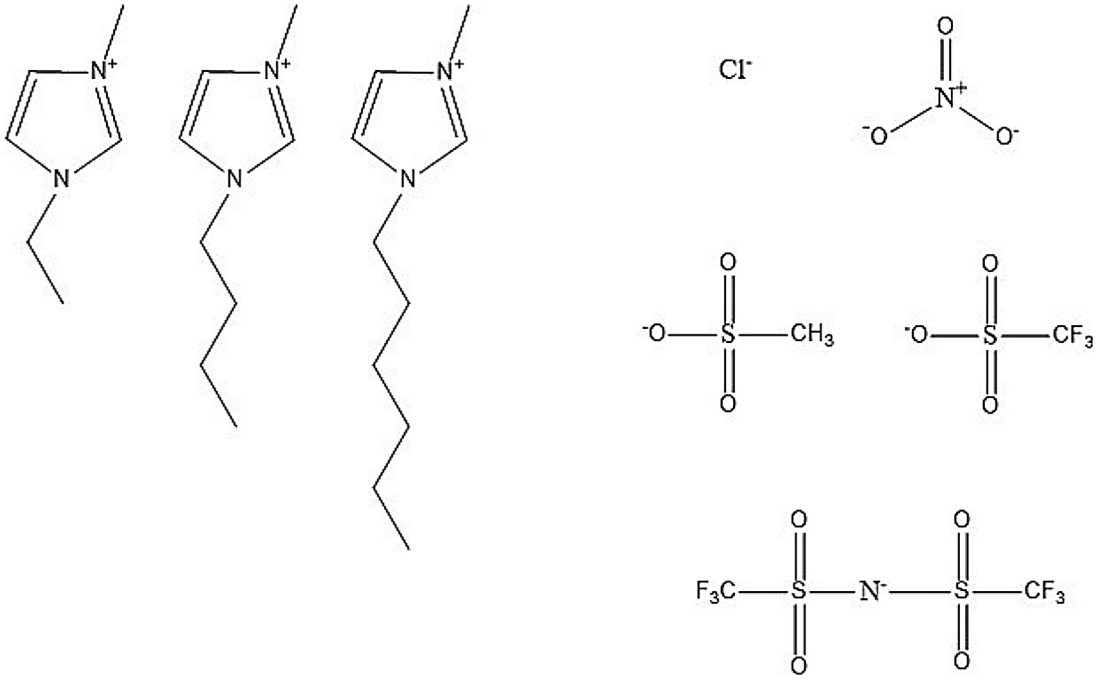

Fig. 1. Chemical structures of the cations and anions used in this work. Cations included 1-ethyl-3-methylimidazolium, [Im_{21}^+], 1-butyl-3-methylimidazolium, [Im_{41}^+], and 1-hexyl-3-methylimidazolium, [Im_{61}^+]. Anions included chloride, nitrate, methanesulfonate [$MeSO_3^-$], trifluoromethanesulfonate [$TFMS^-$], and bis(trifluoromethylsulfonyl)imide [Tf_2N^-].

Table 1
Molecules and Ionic Liquids Studied.

Molecules/ILs[a]	CAS RN[b]	Chemical Name	Source (Purity) [c]
	9002–10-2	Tyrosinase	Sigma Aldrich 50K units
L-dopa	59–92-7	L-3,4-dihydroxylphenylalaine	Sigma Aldrich (98%)
	7778–77-0	Potassium phosphate, monobasic	Fisher (99%)
	16788–57-1	Potassium phosphate, dibasic	Acros (99%)
$[Im_{21}^+][NO_3^-]$	143314–14-1	1-ethyl-3-methylimidazolium nitrate	Fluka (97%)
$[Im_{21}^+][MeSO_3^-]$	516474–01-4	1-ethyl-3-methylimidazolium methanesulfonate	EMD (98%)
$[Im_{21}^+][TFMS^-]$	145022–44-2	1-ethyl-3-methylimidazolium trifluoromethanesulfonate	EMD (98%)
$[Im_{21}^+][Tf_2N^-]$	174899–82-2	1-ethyl-3-methylimidazolium bis(trifluoromethylsulfonyl)imide	EMD (98%)
$[Im_{41}^+][Cl^-]$	79917–90-1	1-butyl-3-methylimidazolium chloride	EMD (98%)
$[Im_{41}^+][MeSO_3^-]$	342789–81-5	1-butyl-3-methylimidazolium methanesulfonate	IoLiTec (95%)
$[Im_{61}^+][Cl^-]$	171058–17-6	1-hexyl-3-methylimidazolium chloride	Solvent Innovation (97%)

[a] Chemical abbreviations.
[b] CAS RN is the chemical abstract registry number.
[c] Manufacturer purity.

4 °C, making only enough solution to insure that none lasted more than two or three days. In this way, we attempted to minimize solution variability resulting from enzyme degradation. IL concentrations were made by micropipetting neat IL to produce solutions that ranged from ~5–250 mM.

The activity assay used for tyrosinase was based on spectrophotometric measurements using a Perkin-Elmer Lambda 800 UV/VIS spectrometer set at 475 nm where we detected the dopaquinone product formation. The reaction was performed in a standard 1 cm path length quartz cuvette (23-Q-10, Starna, Atascadero, CA) with a matched cuvette in the reference channel of the spectrometer that contained a blank solution composed of buffer and ionic liquid to correct the measured absorbance. Prior to a kinetic run, reagent solutions were equilibrated and maintained at 30 °C using a Neslab thermostated chiller. To prepare the reaction mixture, the desired amounts of buffer, IL, and then enzyme solutions were first micropipetted into a cuvette followed by thorough mixing for at least 60 s to ensure solution homogenization. To initiate the reaction, the desired amount of L-dopa was then micropipetted into the cuvette followed by complete cuvette inversions for 2 s, *not* shaking to avoid aerating the solution and creating an emulsion, and then placing the cuvette immediately into the spectrometer and starting the acquisition. This sequence was carefully performed in an effort to be as systematic, consistent, and precise as possible. Absorption data was acquired as a function of reaction time at 475 nm, using 5 s intervals. The rate of dopaquinone formation was derived by using the method of initial rate as defined by the slope of the linear response window of [dopaquinone] versus time plots at early reaction times. Dopaquinone concentrations were calculated directly from absorbance data using the absorptivity value of 3600 M^{-1} cm^{-1} [42].

The tyrosinase/L-dopa system is well-described by Michaelis-Menten kinetics. In this model, the IL inhibition behavior was determined from Lineweaver-Burk (L-B, double reciprocal) plots, $(1/V_0) = (K_m/V_{max})(1/[S]) + 1/V_{max}$ where V_0 is the initial reaction velocity calculated from the absorbance versus time data, K_m is the Michaelis constant, V_{max} is the maximum reaction velocity, and $[S]$ is the substrate concentration [43]. Fits to a linear model allow extraction of the slope ($=K_m/V_{max}$), y-intercept ($1/V_{max}$), and x-intercept ($=-1/K_m$). Assuming a two-step kinetic model, the

product formation rate constant (k_2) is defined as the limiting rate constant of an enzyme-catalyzed reaction (k_{cat}) where $V_{max} = k_2[E]$ and [E] is the enzyme concentration [43]. From the L-B data, we calculated the K_m, k_{cat}, and V_{max} parameters and from these values the $\frac{k_{cat}}{K_m}$ ratio. Finally, we used the neat buffer solution data as a comparator to normalize the IL data and calculated the *relative* activity, $\left(\frac{k_{cat}}{K_m}\right)_{IL} / \left(\frac{k_{cat}}{K_m}\right)_{Buffer}$.

2.2.2. Computational methods

We used Spartan'16® Parallel Suite [44] to compute all ionic liquid parameters. Except for molecular mechanics and semi-empirical models, the calculation methods used in Spartan have been documented elsewhere [45]. In the present work, calculations were performed using the Hartree-Fock 3–21G level of theory and for simulating ions in water the SM8 [46] water model was used. The SM8 water model is an implicit continuum solvation model that estimates the electrostatic polarization of a dielectric medium using bulk solvent properties. For comparison, ion properties were also calculated using DFT theory with the B3LYP functional and 6–31G* basis set. The resulting hydrated ion energies were <1% different than the computed HF 3–21G method so a more sophisticated level of theory was deemed not necessary for the intended purposes in this work. Cation and anion structures were first geometry-optimized to minimize the ion energy, after which electrostatic potentials were determined. The final structures were exported into a Sybyl (.mol2) format in preparation for docking studies.

Ligand docking simulations were performed using the open-source programs for AutoDock4.2 [47] or AutoDock Vina [48] along with AutoDockTools (ADT) [47], a graphical user interface compliment to the AutoDock software suite. AutoDock4.2 uses an AMBER based force field scoring function that estimates the binding free energy of a ligand to its target. Vina was developed as a successor to AutoDock 4.2 and boasts faster, more accurate results with less direct investment required by the end user. Here, we used Vina to perform blind docking simulations by searching the entire tyrosinase structure to find the best docking sites for each of the IL ions. To that end, we performed no less than five independent docking runs and averaged the results of each docking, in sequence, to produce a representative result and the standard deviations associated with these replicate data. At times, the docked energies were identical for the replicates and therefore yielded a standard deviation of zero. In order to run the Vina docking program, both ligand and receptor structures must be first prepared in a specific file format. We used ADT to create the necessary. pdbqt files that are read by Vina. For the tyrosinase receptor, we used the crystallographic structure 4P6S from the RCSB PDB website. To minimize the search area on the receptor we removed chain B from the PDB file. We then removed the two L-dopa molecules that were in chain A to make the active site accessible to docking the IL ions. Ligand (IL ions) structures were directly imported from the Spartan'16 file as described above and the electrostatic charges were preserved. In the simulation ligand positions were initialized with a random starting position.

3. Results and discussion

3.1. Tyrosinase activity in imidazolium ILs

An absorbance data set was collected for kinetics determination that consisted of five L-dopa concentrations (0.5–3.8 mM) in an IL/phosphate buffer solution at various IL concentrations. Fig. 2 presents a representative data set for the tyrosinase/L-dopa reaction the presence of 48 mM $[Im_{21}^+][MeSO_3^-]$. All data sets were created in this way at each IL concentration for the ILs studied here.

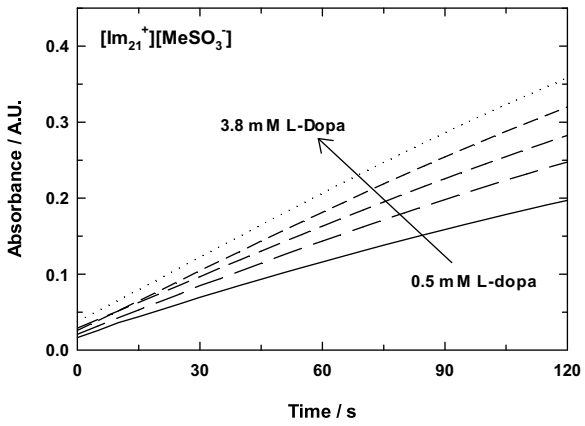

Fig. 2. Absorbance traces for the tyrosinase/L-dopa reaction in 48.3 mM $[Im_{21}^+][MeSO_3^-]$; solution pH = 6.8 and T = 30 °C. The arrow shows the absorbance progression as a function of substrate concentrations at 0.5 mM (solid line), 1.0 mM (long dashes), 1.5 mM (medium dashes), 2.5 mM (short dashes) and 3.8 mM (dotted line) L-dopa.

The initial reaction velocity was calculated from the absorbance data using only data from 10 to 50 s reaction time where the absorbance change was most linear. We examined various time ranges and determined that using data over a longer window introduced absorbance non-linearity. Fig. 3 shows the composite results for the relative activity all systems reported here. Without exception, all cation/anion IL combinations inhibited the tyrosinase relative activity and activity decreased systematically as IL concentration increased. The dotted line indicates 50% relative activity. Table 2 collects the estimated IC_{50} values and these data quantify the inhibition effectiveness for each of the ILs. There a large variation in inhibition by $[Im_{21}^+]$ ILs and the inhibition capacity is strongly influenced by the anion present. The two $[Im_{41}^+]$ ILs display statistically the same level of inhibition. The longest chain cation, $[Im_{61}^+]$ along with $[Im_{21}^+][Tf_2N^-]$ both show substantial capacity for tyrosinase inhibition. We have discussed these observations elsewhere and explained them in the context of anion hydrophobicity and polarization coupled with the increased cation hydrophobic effect [49].

3.2. Inhibition types resulting from IL interactions with mushroom tyrosinase

Having characterized the tyrosinase activity, we then focused on determining the specific mode(s) of inhibition by the imidazolium ILs on tyrosinase. Each of the IL systems presented here were processed as follows. A Lineweaver – Burk (L-B, double reciprocal) plot was generated for the data set, from which we extracted the slope and intercept values that were used to calculate the K_m and V_{max} parameters. This was repeated for each IL concentration used in the system studied. The kinetic data was also used to quantify the equilibrium constant for inhibitor binding. The left panel of Fig. 4 shows an example for a complete set of L-B plots that resulted from the reaction between tyrosinase and L-dopa in the presence of $[Im_{21}^+][MeSO_3^-]$/phosphate buffer solution at pH = 6.8 and T = 30 °C. The series of $[Im_{21}^+][MeSO_3^-]$ concentrations shown here are 4.8 (●), 24.1 (○), 38.6 (▼), 48.3 (△), and 62.8 (■) mM. The individual regression lines are fits to the linear model (see Methods section). Figs. S1–S5 in supporting information shows L-B plots for the remaining ILs. Each of these data sets were reasonably well described by a linear fit with $r^2 > 0.95$, which was a typical fitting result for all ILs studied in this work. The right panel shows two secondary plots for the L-B slope and L-B intercept that were used to

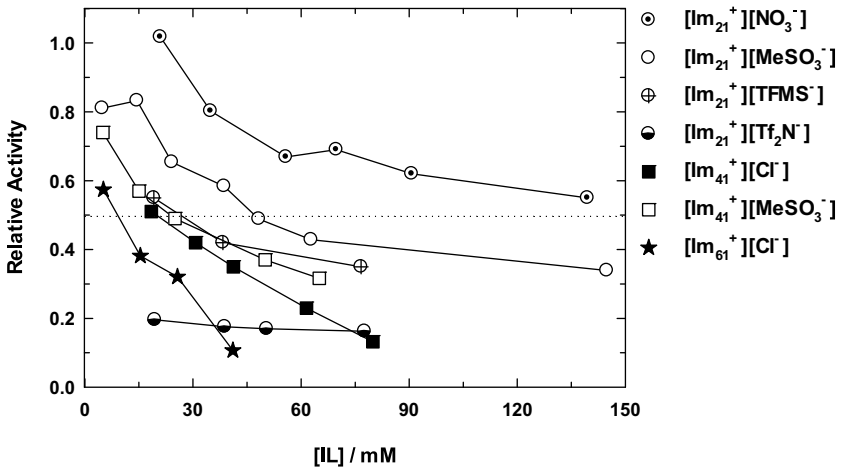

Fig. 3. Tyrosinase relative activity in the presence of various ionic liquid concentrations at 30 °C. Solid lines are included as a visual aid to distinguish the various IL data sets. Symbols are organized by cation identity with circles = [Im_{21}^+], squares = [Im_{41}^+], and stars = [Im_{61}^+]. The horizontal dotted line marks the 50% relative activity line.

Table 2
Inhibition Data for Mushroom Tyrosinase in Ionic Liquids.

Ionic Liquid	IC_{50} [a] / mM	Type	K_{EI} [b] / mM	K_{EIS} [b] / mM	Ratio
[Im_{21}^+][NO_3^-]	180 ± 20	mixed	43 ± 18	126 ± 29	2.9
[Im_{21}^+][$MeSO_3^-$]	54 ± 9	mixed	22 ± 7	62 ± 9	2.8
[Im_{21}^+][$TFMS^-$]	24 ± 4	mixed	24 ± 12	37 ± 17	1.5
[Im_{21}^+][Tf_2N^-]	–	competitive	0.7 ± 0.1	483 ± 93	656
[Im_{41}^+][Cl^-]	20 ± 3	mixed	43 ± 10	110 ± 40	2.5
[Im_{41}^+][$MeSO_3^-$]	22 ± 2	mixed	7 ± 4	77 ± 17	11.
[Im_{61}^+][Cl^-]	9 ± 1	mixed	3.8 ± 0.5	8.9 ± 0.9	2.3

[a] Estimates of these values were obtained by regressing the relative activity data and computing the corresponding 50% activity value from the regression equation.
[b] Binding equilibrium constant values were calculated from Lineweaver-Burk slopes and intercepts. [c]Ratio = K_{EIS}/K_{EI}.

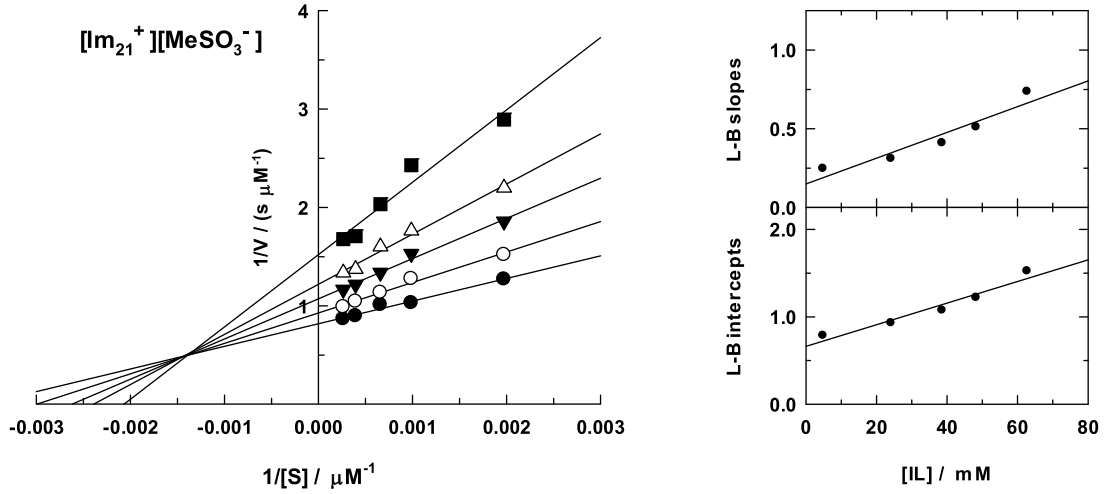

Fig. 4. Left panel: Series of Lineweaver-Burk (L-B, double reciprocal) plots for mushroom tyrosinase/L-dopa reactions in solutions of [Im_{21}^+][$MeSO_3^-$]/phosphate buffer held at pH = 6.8 and T = 30 °C. [Im_{21}^+][$MeSO_3^-$] concentrations are 4.8 (●), 24.1 (○), 38.6 (▼), 48.3 (△), and 62.8 (■) mM. The regression lines are fits to a linear model, all $r^2 > 0.95$. Right panels: plots of slopes and intercepts recovered from the Lineweaver-Burk plot regression calculations. L-B slopes and intercepts were used to calculate K_{EI} and K_{EIS} inhibition equilibrium constants, respectively.

extract equilibrium constants (see Section 3.2.1 below for details) [8,50].

3.2.1. *Inhibition kinetics for tyrosinase activity in [Im_{21}^+] ILs*

In the Michaelis-Menten kinetic scheme for enzyme inhibition, the type of inhibition that governs the enzyme reaction is readily recognizable by the pattern of resulting lines from a series of L-B plots [43]. For plots that show a set of lines intersecting at the y-intercept, this is indicative of a competitive inhibition model whereas a non-competitive or mixed inhibition model is revealed by plots with lines that intersect in the second quadrant. The data for [Im_{21}^+][$MeSO_3^-$] shown in Fig. 4 is consistent with the latter model, mixed inhibition. In addition to the L-B plots for this IL, further supporting evidence for mixed inhibition came from the observation that the as the IL concentration increased, the K_m values increased while simultaneously the V_{max} values decreased. From these data, we concluded that the [Im_{21}^+][$MeSO_3^-$] inhibitor (I) is able to bind not only to free tyrosinase (E) to make the

enzyme-inhibitor (EI) complex, but also to the tyrosinase-L-dopa (ES*) complex to form the enzyme-substrate-inhibitor (ESI*) complex. We calculated the equilibrium binding constants for each of these cases. For the (EI) complex, the slopes from each of the L-B fits were used to make a secondary plot of L-B slope as a function of IL concentration (see the upper graph, right panel of Fig. 4). These data were regressed using a linear model to extract the x-intercept, which directly yields the (EI) equilibrium binding constant (K_{EI}) [8,50]. Similarly, to calculate the (ESI*) equilibrium binding constant (K_{ESI}) the L-B intercepts were plotted as a function of [IL] concentration (see the lower graph, right panel of Fig. 4). The values of K_{EI} and K_{EIS} for $[Im_{21}^+][MeSO_3^-]$ binding were 22 ± 7 and 62 ± 9 mM, respectively, and are reported in Table 2. We observed similar behavior for $[Im_{21}^+][NO_3^-]$ and $[Im_{21}^+][TFMS^-]$ in that for both of these cases, the ILs also displayed mixed inhibition characteristics with K_{EI} and K_{EIS} reported in Table 2. It is noteworthy that $[Im_{21}^+][NO_3^-]$ has binding equilibrium constants that are at least twice that of the two methanesulfonate-based ILs. Larger values of K are indicative of *weaker* inhibitor binding and this observation is consistent with the relative activity behavior where $[Im_{21}^+][NO_3^-]$ has the least inhibitory effect on tyrosinase at any given IL concentration [49]. Similarly, we can assess the binding affinity preference of the ILs for either free or substrate-bound enzyme by examining the K_{EIS}/K_{EI} ratios reported in Table 2. Since each of the K_{EIS}/K_{EI} ratios are greater than 1 for these three ILs, this indicates that they have a binding preference for free enzyme over the ES* complex. But we also point out that the preference for free enzyme weakens as anion hydrophobicity increases.

Of particular interest in these experiments is the behavior of tyrosinase with $[Im_{21}^+][Tf_2N^-]$, which is markedly different from all other ILs. Fig. 5 shows the L-B plots for the tyrosinase/L-dopa kinetics that were measured using three $[Im_{21}^+][Tf_2N^-]$ concentrations. In consideration of the inhibition type, this data suggests that the L-B regression lines intersect on the 1/V axis and thus is characteristic of competitive inhibition. Compared to the other $[Im_{21}^+]$ ILs, here the apparent K_m values increase while V_{max} remains effectively constant to within experimental uncertainty (data not shown). As described above, we calculated the corresponding K_I value for the interactions between this IL and tyrosinase using the L-B slopes and computed a value of 0.7 mM, see Table 2. This K_I value represents a significant increase in the IL affinity for tyrosinase, an increase in excess of 30 times greater than $[Im_{21}^+][MeSO_3^-]$ and $[Im_{21}^+][TFMS^-]$ and about 60 times greater than $[Im_{21}^+][NO_3^-]$. Comparing all of the $[Im_{21}^+]$ ILs, there is a clear pattern of binding to tyrosinase that appears to follow the anion hydrophobicity and polarizability. Of these four anions, ranking by hydrophobicity results in the sequence of these ions as $[NO_3^-] < [MeSO_3^-] < [TFMS^-] <$ and $[Tf_2N^-]$, thus it was not unanticipated that $[Tf_2N^-]$ preferred the relative hydrophobicity of the enzyme compared to the phosphate buffer. Moreover, two recent reviews have discussed the idea that anions are reported to have a more active role in enzyme activity/stability through greater polarizability effects relative to cations [35,51], which is consistent with our observations in $[Im_{21}^+]$ ILs.

3.2.2. Inhibition kinetics for tyrosinase activity in $[Im_{41}^+]$ and $[Im_{61}^+]$ ILs

The results from all of the kinetic measurements for the $[Im_{41}^+]$ and $[Im_{61}^+]$ ILs are also summarized in Table 2. From these data, we briefly highlight several features for the C_4 and C_6 alkyl chain imidazolium derivatives. For the two $[Im_{41}^+]$ ILs, their behavior parallels that observed for the $[Im_{21}^+]$ ILs. Several specific points are apparent from these data. First, the IC_{50} data show that the presence of a longer alkyl chain on the imidazolium cation contributes significantly to the inhibition of tyrosinase, by a factor of ~2.5 on going from $[Im_{21}^+][MeSO_3^-]$ to $[Im_{41}^+][MeSO_3^-]$. The increased hydrophobic character of the IL enhances the hydrophobic effect on the tyrosinase [34,35,38]. Second, the L-B plots for these $[Im_{41}^+]$ ILs (not shown) both indicate mixed type inhibition since the family of lines intersects in the second quadrant of the graph. Third, similar to the $[Im_{21}^+]$ ILs, the K_{EI} and K_{EIS} values show that binding with free enzyme is preferred over the ES* complex and K_{EIS}/K_{EI} ratios. Fourth, the $[MeSO_3^-]$ binds more tightly to free tyrosinase compared to Cl^-, by roughly a factor of six whereas in the ES* complex the preferential binding is less than a factor of two.

3.2.3. Inhibition kinetic parameters for tyrosinase activity in $[Im_{61}^+]$ ILs

Although we only measured one $[Im_{61}^+]$ IL, we can comment on the cation effect by comparing to the $[Im_{41}^+][Cl^-]$ data. Increasing the chain length to C_6 has the expected effect of lowering the IC_{50} and decreasing the binding equilibrium constants. It appears that increasing the imidazolium alkyl chain by only two carbons plays a substantial role in the ensuing inhibition of tyrosinase, presumably through increased screening of the hydrophobic effect [34]. While the K_{EIS}/K_{EI} ratios for $[Im_{41}^+][Cl^-]$ and $[Im_{61}^+][Cl^-]$ are statistically identical, the absolute magnitudes of K_{EI} and K_{EIS} are quite different, by a factor of ~11. This suggests that when bound, the effect of $[Im_{41}^+]$ and $[Im_{61}^+]$ on tyrosinase and the ES* complex is likely very similar for the two cations, however the difference in the binding affinities is large with $[Im_{61}^+]$ being more strongly bound to both the free enzyme and the ES* complex.

3.3. Molecular docking simulations

To aid experimental work, molecular docking simulations have been used as a tool to augment the molecular level interpretation of the data. A number of recent articles that discussed tyrosinase inhibition [22,52–61] and protein-IL interactions [26,32,60,62–64] have demonstrated the applicability of including docking simulations in estimating potential sites for ligand binding.

While the experimental kinetic results provides compelling evidence to support mixed inhibition kinetics in all but $[Im_{21}^+][Tf_2N^-]$ (competitive inhibition) and yield estimates of binding equilibrium constants for IL binding to free tyrosinase and the ES* complex, there is at least one other point of consideration that we now address. Up to this point, we have not probed in any depth potential sites within tyrosinase where IL ions might bind, either the active site directly or associations with residues outside of the active site that contribute to governing the tyrosinase activity. In an effort to seek a molecular explanation for the observed inhibition behavior of the ILs used here, we undertook a series of molecular docking studies using AutoDock4.2 and AutoDock Vina. The calculated dockings were in general agreement between both programs but Vina is reported to be more accurate [48] so we report the results from that data. Docking calculations were performed using L-dopa as a means of testing the agreement between Vina dockings and the reported crystal structure for 4P6S [12]. The lowest energy docking configuration for L-dopa (-6.3 kcal/mol) is in good agreement with experiment and places the L-dopa in proximity of HIS208, VAL217, VAL218, ALA221, and the HIS60-bound metal atom. The amino acids that compose the A-chain tyrosinase binding pocket for L-dopa are shown in Fig. 6. The importance of free histidine residues for ligand binding has been discussed and linked to tyrosinase performance [55] and we note that this idea is consistent with most of the docking sites that resulted from our studies here. Any of the active site interactions between IL ions and tyrosinase in our results included the metal-free HIS208 in most cases.

Data for the top nine docking results for each ion used in this work were thoroughly reviewed. We hasten to add a cautionary note here that care must be taken to avoid over-interpreting differences in docking energies. While it is no doubt customary to

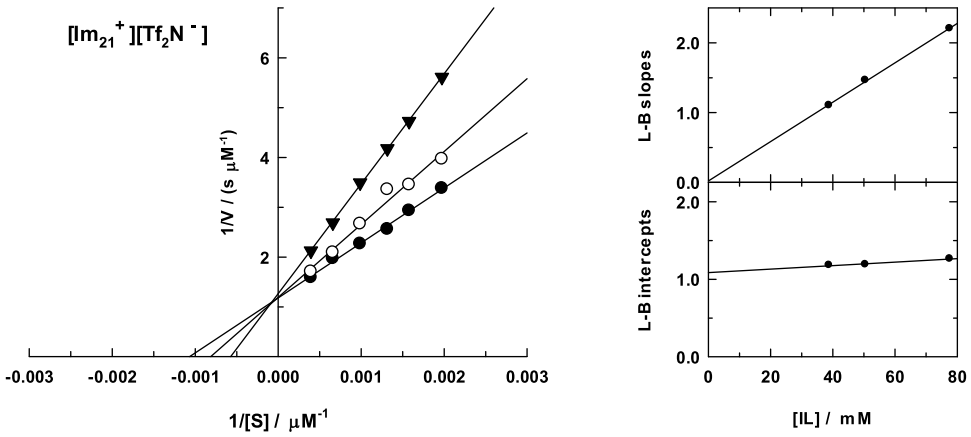

Fig. 5. Left panel: Series of Lineweaver-Burk (L-B, double reciprocal) plots for mushroom tyrosinase/L-dopa reactions in solutions of $[Im_{21}^+][Tf_2N^-]$/phosphate buffer at pH = 6.8 and T = 30 °C. $[Im_{21}^+][Tf_2N^-]$ concentrations are 38.8 (●), 50.4 (○), and 77.6 (▼) mM. The regression lines are fits to a linear model, all $r^2 > 0.98$. Right panel: slopes recovered from the Lineweaver-Burk plot regression calculations and used to calculate the K_{EI} inhibition equilibrium constants.

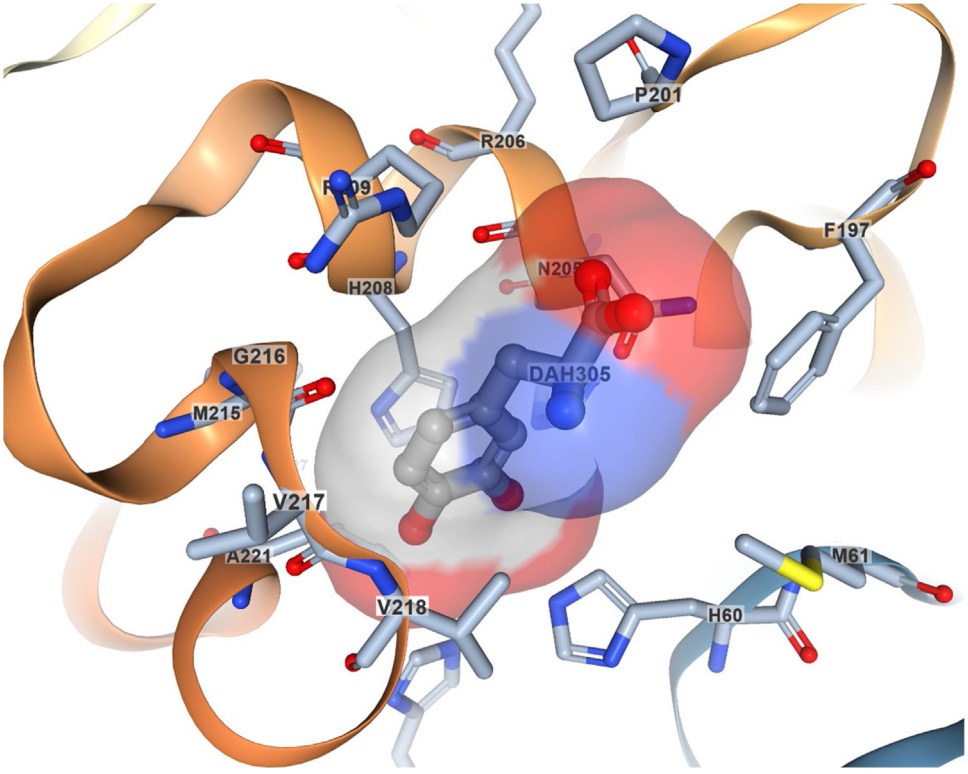

Fig. 6. Amino acids that compose the binding pocket (active site) for L-dopa (DAH305), image taken from PDB structure 4P6S [12].

Table 3
Molecular Docking Data Ionic Liquid Ions in Mushroom Tyrosinase.

Ionic Liquid	Energy / kcal mol^{-1}	|deviation| [a] / kcal mol^{-1}	Location [b]	Specific Interactions
L-dopa	−5.83 ± 0.37		A.S.	–
$[Im_{21}^+]$	−4.38 ± 0.22	0.7	A.S.	π-π (HIS208)
$[Im_{41}^+]$	−4.63 ± 0.26	0.6	A.S.	π-π (HIS208)
$[Im_{61}^+]$	−5.02 ± 0.20	0.8	A.S.	π-π (HIS208)
$[NO_3^-]$	−3.05 ± 0.07	0.4	HIS231	H-bond (HIS231)
$[MeSO_3^-]$	−2.82 ± 0.09	0.4	A.S.	–
$[TFMS^-]$	−4.27 ± 0.07	0.2	A.S.	–
$[Tf_2N^-]$	−5.22 ± 0.14	0.3	A.S.	—

[a] Absolute deviation between the maximum and minimum docked energy values that were associated with the top docking locations.
[b] Most probable location of the primary docking answer. See text for additional docking location results. The abbreviation "A.S." represents active site interactions.

Please cite this article in press as: M.P. Heitz, J.W. Rupp, Int. J. Biol. Macromol. (2017), https://doi.org/10.1016/j.ijbiomac.2017.10.066

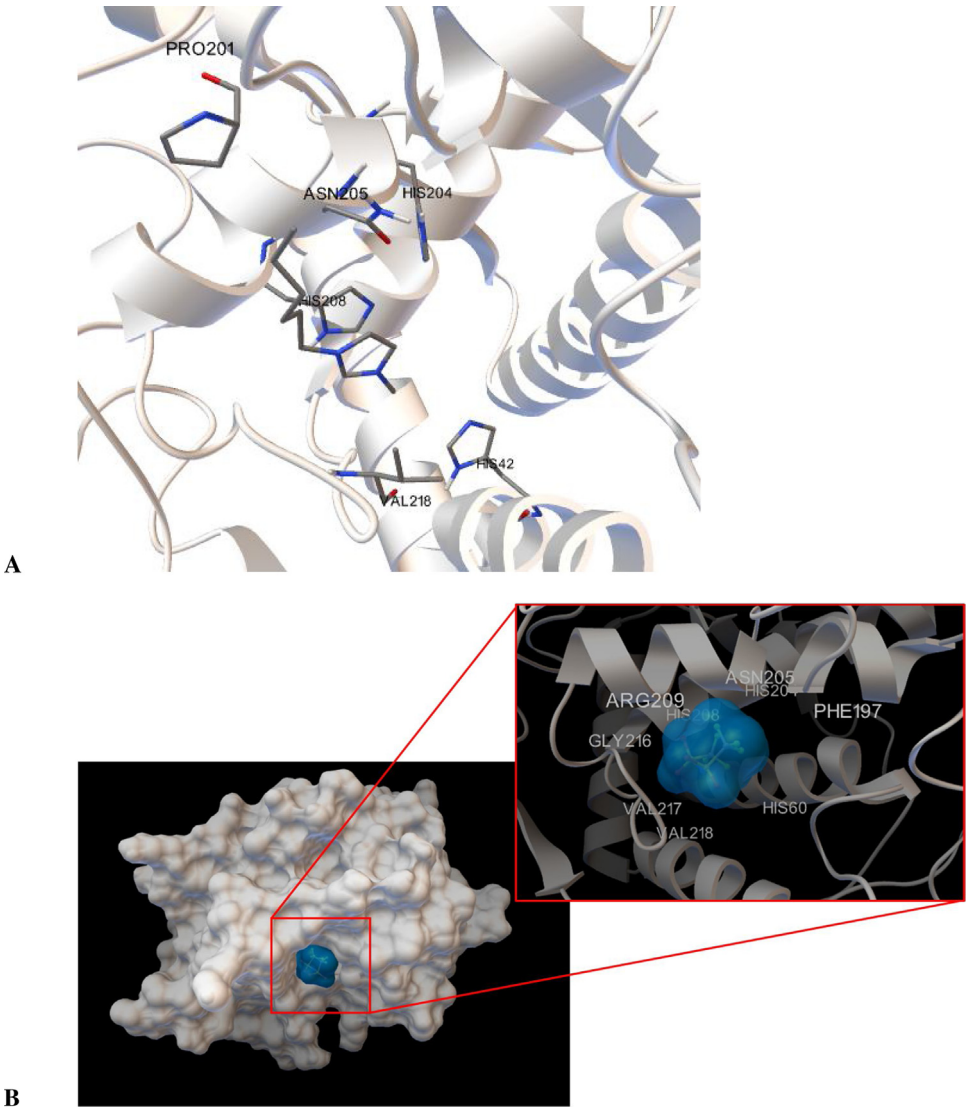

Fig. 7. Computational docking example results (from AutoDock Vina) for IL ion binding to mushroom tyrosinase. Panel A: lowest energy docking location for [Im_{61}^+], which occurred in the tyrosinase active site (see Fig. 6). Also shown are the computed nearest neighbor residues for [Im_{61}^+] that include (from top to bottom in the figure): PRO201, HIS204, ASN205, HIS208, VAL218, and HIS42. Panel B: image of the lowest energy docking for [Tf_2N^-], which was in the tyrosinase active site. Nearest neighbor residues are shown in the zoomed image and include (moving clockwise): ARG209, HIS208, ASN205, HIS204, PHE197, HIS60, VAL218, VAL217, GLY216.

report only the primary docking result, perhaps a better representation of the most probable ligand binding is likely represented by an average of the top several docking sites. This is particularly true for top dockings that differ by less than 0.5 kcal/mol, considering that $RT \approx 0.5$ kcal/mol and thermal randomization alone can influence the true docking site/orientation. As part of our evaluation of docking results we also considered the energy range of top results when selecting which dockings best represent chemical intuition. So with these points in mind, the binding energies calculated by averaging the three lowest energy dockings for the [$Im_{x,1}^+$] cations and their associated standard deviations are reported in Table 3. The [Im_{21}^+] results from the top three dockings across five replicates showed an absolute energy difference of only 0.4 kcal/mol. This small difference, given the 0.2 kcal/mol uncertainty, justified averaging of these data. Moreover, for [Im_{21}^+] the top nine docking site energies ranged from −4.6 to −3.6 kcal/mol, only a 20% overall change. The [Im_{41}^+] and [Im_{61}^+] ions showed similar results and were treated accordingly. We note that for all the imidazolium cations, the primary docking location was always the tyrosinase active site. As an example, we show the docked position of [Im_{61}^+] along with the identified nearest tyrosinase residues as determined from a close contact radius of 4 Å in Fig. 7, panel A. Dockings for [Im_{21}^+] and [Im_{41}^+] are shown in supporting information, Figs. S6 and S7, respectively. Residues common to all cation dockings were HIS204, ASN205, HIS208, and VAL218. Regardless of the alkyl chain on the imidazole ring all of the cations clearly showed π-π interactions with HIS208. Some of the higher energy docking orientations also suggested that there were π-π interactions with HIS204. In all of the [$Im_{x,1}^+$] dockings, the differences in the docked results stemmed only from orientation arrangements of the cation within the active site. According to the energies, [Im_{61}^+] showed the strongest interaction with tyrosinase by about 0.6 kcal/mol compared to [Im_{21}^+]. We note that the collective cation data suggests a very small but systematic decrease in energy on going from C_2 to C_6, which is likely reflective of the longer alkyl chain having additional van der Waals interactions with the enzyme. Moreover, for the longer alkyl chains conformational flexibility can easily be the source of variation in different docking answers. We observed this behavior in each of the cation results, but in particular with dockings for [Im_{61}^+] because of the torsional flexibility of the C_6 chain. Since the top six docking locations for all cations are found in the

Please cite this article in press as: M.P. Heitz, J.W. Rupp, Int. J. Biol. Macromol. (2017), https://doi.org/10.1016/j.ijbiomac.2017.10.066

active site, it appears that the enzyme-anion interactions play a more significant role in the observed variation in tyrosinase relative activity.

Docking results for the anions used here are collected in Table 3 and arranged in order of the increased impact on tyrosinase relative activity. We were unable to perform dockings for Cl^- because the pdbqt file preparation required a torsion tree root, which apparently cannot be created for a monatomic ion. To provide a space-filling perspective we show a molecular surface image [65] in Fig. 7, panel B, for the lowest energy [Tf_2N^-] docking. Remaining anion docking images are shown in Figs. S8–S10 of the supporting information. For all docking in the active site, the ion fills the pocket and effectively blocks access to L-dopa accounting for the competitive portion of the mixed inhibition. Except for [NO_3^-], the lowest energy docking location was in the L-dopa active site for all of the anions used here.

3.3.1. [NO_3^-] dockings

The Vina results suggested for [NO_3^-] placed this ion at HIS231 with a 1.83 Å hydrogen-bond formed between the [NO_3^-] oxygen and the imidazole hydrogen. The bond energy was reported as −7.6 kcal/mol. Active site dockings were also reported in replicate runs with identical scores (ion binding energies) so evidently the most probable location for [NO_3^-] is better thought of as a distribution of equal energy locations. If [NO_3^-] is equally likely to bind in a non-active site location then this explains the observation that [NO_3^-] has the least impact on tyrosinase relative activity, particularly at low [NO_3^-] concentrations. Moreover, for the active site dockings, no hydrogen bonding was observed. Other dockings for [NO_3^-] also included ARG6 and ARG78, each of which displayed two hydrogen bonds of 2.0 ± 0.1 Å.

3.3.2. [$MeSO_3^-$] dockings

As mentioned above, the primary docking location for [$MeSO_3^-$] was the L-dopa active site and this was consistent over all replicate docking runs. There were two other reproducible locations identified by Vina that produced energies within 0.2 kcal/mol of the lowest energy position. The second most consistent docking set involved LYS19, SER110 AND GLN107. Interactions with these residues included increased stabilization through hydrogen bond formation with GLN107 and with SER110. The third preferred docking was with ARG6 and ARG78, similar to [NO_3^-] in both location and the presence of hydrogen bonding interactions with the [$MeSO_3^-$] oxygen atoms. Distances here were of comparable lengths, at 2.0 ± 0.1 Å. In the relative activity context for the [Im_{21}^+] set of ILs, [$MeSO_3^-$] ranked as the second *least* effective tyrosinase inhibition. Finally, for this anion, we also note that when the cation dockings were also considered alongside this anion's dockings the more effective tyrosinase inhibition by [Im_{41}^+][$MeSO_3^-$] over [Im_{21}^+][$MeSO_3^-$] is clearly consistent with 1) the lower energy [Im_{41}^+] docking value and 2) the fact that even though [$MeSO_3^-$] also docks outside of the L-dopa active site, the more strongly bound [Im_{41}^+] docking in the active site had a greater influence on tyrosinase inhibition.

3.3.3. [$TFMS^-$] dockings

From a structural perspective, [$TFMS^-$] is nearly identical to [$MeSO_3^-$] with the exception of the perfluorinated methyl moiety and therefore one might predict this ion should behave very similarly to [$MeSO_3^-$]. However, the data showed that all of the top docking locations were localized in the L-dopa active site in each of the replicate runs. In only one of the five runs performed for this ion did the top three docking positions vary; that is, 1 in 15 runs produced a location variant. As one might anticipate, this additional docking site was at the LYS19, SER110 AND GLN107 residues, similar to that observed for [$MeSO_3^-$]. Of these two anions, we also note that [$TFMS^-$] was a stronger inhibitor of the tyrosinase relative activity (see comparable data for [Im_{21}^+] in Fig. 3 and Table 2). The docking energy for [$TFMS^-$] was significantly less than [$MeSO_3^-$], by 1.4 kcal/mol, indicating stronger binding of this fluorinated anion by tyrosinase.

3.3.4. [Tf_2N^-] dockings

All docking locations for [Tf_2N^-] were in the L-dopa active site. This result was consistent for all runs and for all nine results, although for consistency the reported energy in Table 3 is only for the average of the top three dockings from the replicate runs. Of all anions studied here, [Tf_2N^-] was by far the most consistent with respect to location. Only the relative orientation of the anion changed among all of the dockings. The larger variation in docking energy is likely caused by the presence of highly electronegative atoms (N, O, F, and S) that compose this anion and therefore dominate the resulting set of interactions with the residues in the binding pocket.

4. Summary and conclusions

The myriad of ion combinations that can be used to form ILs offers a nearly limitless set of choices for designing task-specific systems. In this work we focused on the enzymatic activity of the type 3[12] copper-containing oxidase mushroom tyrosinase and the inhibition of activity alkylimidazolium ionic liquids. On the whole, this work demonstrates the ability to use a small set of imidazolium ILs to inhibit mushroom tyrosinase activity towards the L-dopa substrate. Both the choice of ion identity and concentration serve as an effective combination with which one can selectively tailor tyrosinase inhibition.

We have presented experimental data that characterized the relative activity of this enzyme using the substrate L-dopa in phosphate buffer solution at pH = 6.8 and T = 30 °C using Michaelis-Menten kinetic parameters to determine the enzymatic activity. We calculated the *relative* activity as the ratio of (activity in the presence of ILs)/(activity in buffer) and found that the relative activity varied from about 15–95% over a small IL concentration window of ∼10–100 mM. From the kinetic data, we determined the inhibition type for the IL/tyrosinase system. In all solutions, the presence of ILs resulted in mixed type inhibition with the exception of [Im_{21}^+][Tf_2N^-], which showed only competitive inhibition.

Our experimental results showed increased inhibition of tyrosinase activity in the presence of the [Im_{x1}^+] ILs in proportion to cation alkyl chain length, and followed the sequence [Im_{21}^+] < [Im_{41}^+] < [Im_{61}^+], consistent with literature reports [27,34,36,66,67]. The increased inhibition is connected to the increased cation hydrophobicity. Molecular docking studies with AutoDock Vina were used to reveal a set of most probable locations within tyrosinase that accommodated these cations. Without exception, the cations all docked in the L-dopa active site of the enzyme. The binding energies associated with the cation dockings approached the L-dopa energy as alkyl chain length increased. The [Im_{61}^+] energy was within 0.8 kcal/mol and slightly less than the L-dopa energy. Moreover, the cation dockings all formed π-interactions between the imidazole ring and the HIS208 residue. From this data, we concluded that the presence of [$Im_{x,1}^+$] cations created a competitive binding environment for the active site in mushroom tyrosinase.

Docking results showed that it was the IL anions that governed whether the observed IL inhibition was overall competitive. The smaller, less polarizable anions were at least as likely to bind to tyrosinase residues that were outside of the L-dopa active site, which allowed for a cation/anion combination that resulted in mixed inhibition behavior. As the anion size and polarization

Please cite this article in press as: M.P. Heitz, J.W. Rupp, Int. J. Biol. Macromol. (2017), https://doi.org/10.1016/j.ijbiomac.2017.10.066

increased, we observed a concomitant increased in tyrosinase inhibition. Additionally, the extent of halogenation as it governs anion polarization changes also appeared to offer a convenient characterization scheme to explain the observed experimental anion inhibition effect. ILs results based on the [Im_{21}^+] cation showed an increased inhibition trend that followed the sequence [NO_3^-] < [$MeSO_3^-$] < [$TFMS^-$] < [Tf_2N^-]. Docking results for these anions showed that the latter two anions were docked primarily in the L-dopa active site, whereas [NO_3^-] and [$MeSO_3^-$] offered locations that were both in the active site but also in several other locations outside of the active site.

Acknowledgements

The authors gratefully acknowledge support from The College at Brockport, SUNY through the scholarly incentive and Provost post-tenure grant programs.

The authors declare no competing interests.

References

[1] A. Korner, J. Pawelek, Mammalian tyrosinase catalyzes three reactions in the biosynthesis of melanin, Science 217 (4565) (1982) 1163–1165.
[2] B.A. Gilchrest, F.B. Blog, G. Szabo, Effects of aging and chronic sun exposure on melanocytes in human skin, J. Invest. Dermatol. 73 (2) (1979) 141–143.
[3] T.-I. Kim, J. Park, S. Park, Y. Choi, Y. Kim, Visualization of tyrosinase activity in melanoma cells by a BODIPY-Based fluorescent probe, Chem. Commun. 47 (47) (2011) 12640–12642.
[4] A. Sánchez-Ferrer, J. Neptuno Rodríguez-López, F. García-Cánovas, F. García-Carmona, Tyrosinase: a comprehensive review of its mechanism, Biochim. Biophys. Acta (BBA) Prot. Struct. Mol. Enzymol. 1247 (1) (1995) 1–11.
[5] K. Jones, J. Hughes, M. Hong, Q. Jia, S. Orndorff, Modulation of melanogenesis by aloesin: a competitive inhibitor of tyrosinase, Pigment Cell Res. 15 (5) (2002) 335–340.
[6] V.J. Hearing, M. Jiménez, Mammalian tyrosinase–The critical regulatory control point in melanocyte pigmentation, Int. J. Biochem. 19 (12) (1987) 1141–1147.
[7] H. Ando, H. Kondoh, M. Ichihashi, V.J. Hearing, Approaches to identify inhibitors of melanin biosynthesis via the quality control of tyrosinase, J. Invest. Dermatol. 127 (4) (2007) 751–761.
[8] Y.-F. Lin, Y.-H. Hu, H.-T. Lin, X. Liu, Y.-H. Chen, S. Zhang, Q.-X. Chen, Inhibitory effects of propyl gallate on tyrosinase and its application in controlling pericarp browning of harvested longan fruits, J. Agric. Food Chem. 61 (11) (2013) 2889–2895.
[9] K. Lerch, Tyrosinase: molecular and active-Site structure, enzymatic browning and its prevention, Am. Chem. Soc. (1995) 64–80.
[10] G. Battaini, E. Monzani, L. Casella, E. Lonardi, A.W.J.W. Tepper, G.W. Canters, L. Bubacco, Tyrosinase-Catalyzed oxidation of fluorophenols, J. Biol. Chem. 277 (47) (2002) 44606–44612.
[11] J.P. Germanas, S. Wang, A. Miner, W. Hao, J.M. Ready, Discovery of small-Molecule inhibitors of tyrosinase, Bioorg. Med. Chem. Lett. 17 (24) (2007) 6871–6875.
[12] M. Goldfeder, M. Kanteev, S. Isaschar-Ovdat, N. Adir, A. Fishman, Determination of tyrosinase substrate-Binding modes reveals mechanistic differences between type-3 copper proteins, Nat. Commun. 5 (2014) 1–5.
[13] J.F. Wishart, Energy applications of ionic liquids, Energy Environ. Sci. 2 (9) (2009) 956–961.
[14] D.R. MacFarlane, N. Tachikawa, M. Forsyth, J.M. Pringle, P.C. Howlett, G.D. Elliott, J.H. Davis, M. Watanabe, P. Simon, C.A. Angell, Energy applications of ionic liquids, Energy Environ. Sci. 7 (1) (2014) 232–250.
[15] N.V. Plechkova, K.R. Seddon, Applications of ionic liquids in the chemical industry, Chem. Soc. Rev. 37 (1) (2008) 123–150.
[16] M. Zakrewsky, K.S. Lovejoy, T.L. Kern, T.E. Miller, V. Le, A. Nagy, A.M. Goumas, R.S. Iyer, R.E. Del Sesto, A.T. Koppisch, D.T. Fox, S. Mitragotri, Ionic liquids as a class of materials for transdermal delivery and pathogen neutralization, conductimetric determination of thermodynamic pairing constants for symmetrical electrolytes, Proc. Nat. Acad. Sci. 111 (37) (2014) 13313–13318.
[17] D. Subramanian, K. Wu, A. Firoozabadi, Ionic liquids as viscosity modifiers for heavy and extra-Heavy crude oils, Fuel 143 (2015) 519–526.
[18] Ionic Liquids, Industrial Applications for Green Chemistry, American Chemical Society, Washington, DC, 2002.
[19] N. Perez-Pimienta, V.S. Thompson, K. Tran, T. Ponce-Noyola, V. Stavila, S. Singh, B.A. Simmons, Ternary ionic liquid–water pretreatment systems of an agave bagasse and municipal solid waste blend, Biotechnol. Biofuels 10 (1) (2017) 72.
[20] J. Pernak, M. Niemczak, K. Materna, K. Marcinkowska, T. Praczyk, Ionic liquids as herbicides and plant growth regulators, Tetrahedron 69 (23) (2013) 4665–4669.
[21] O.A. Cojocaru, J.L. Shamshina, G. Gurau, A. Syguda, T. Praczyk, J. Pernak, R.D. Rogers, Ionic liquid forms of the herbicide dicamba with increased efficacy and reduced volatility, Green Chem. 15 (8) (2013) 2110–2120.
[22] M.M. Trush, I.V. Semenyuta, S.I. Vdovenko, S.P. Rogalsky, E.O. Lobko, L.O. Metelytsia, Synthesis, spectroscopic and molecular docking studies of imidazolium and pyridinium based ionic liquids with HSA as potential antimicrobial agents, J. Mol. Struct. 1137 (2017) 692–699.
[23] F. Stein, U. Kragl, Biocatalytic reactions in ionic liquids, in: N.V. Plechkova, K.R. Seddon (Eds.), Ionic Liquids Further UnCOILed, John Wiley & Sons, Inc, 2014, pp. 193–216.
[24] U. Kragl, M. Eckstein, N. Kaftzik, Biocatalytic reactions in ionic liquids, in: P. Wasserscheid, T. Welton (Eds.), Ionic Liquids in Synthesis, Wiley-VCH Verlag GmbH & co KGaA, Weinheim, 2003, pp. 336–347.
[25] P. Xu, G.-W. Zheng, P.-X. Du, M.-H. Zong, W.-Y. Lou, Whole-Cell biocatalytic processes with ionic liquids, ACS Sustain. Chem. Eng 4 (2) (2016) 371–386.
[26] R. Patel, M. Kumari, A.B. Khan, Recent advances in the applications of ionic liquids in protein stability and activity: a review, the effect of trifluoroethanol on tyrosinase activity and conformation: inhibition kinetics and computational Simulations, Appl. Biochem. Biotechnol. 172 (8) (2014) 3701–3720.
[27] S. Weibels, A. Syguda, C. Herrmann, H. Weingartner, Steering the enzymatic activity of proteins by ionic liquids. a case study of the enzyme kinetics of yeast alcohol dehydrogenase, Phys. Chem. Chem. Phys. 14 (13) (2012) 4635–4639.
[28] R. Biczak, B. Pawłowska, P. Bałczewski, P. Rychter, The role of the anion in the toxicity of imidazolium ionic liquids, J. Hazard. Mater. 274 (2014) 181–190.
[29] B. Peric, J. Sierra, E. Martí, R. Cruañas, M.A. Garau, A comparative study of the terrestrial ecotoxicity of selected protic and aprotic ionic liquids, Chemosphere 108 (2014) 418–425.
[30] B. Yoo, B. Jing, S.E. Jones, G.A. Lamberti, Y. Zhu, J.K. Shah, E.J. Maginn, Molecular mechanisms of ionic liquid cytotoxicity probed by an integrated experimental and computational approach, carbonate doping in tio2 microsphere: the key parameter influencing others for efficient dye sensitized solar cell, Sci. Rep. 6 (2016) 19889.
[31] T.P. Thuy Pham, C.-W. Cho, Y.-S. Yun, Environmental fate and toxicity of ionic liquids: a review, Water Res. 2 (2010) 352–372.
[32] K.S. Egorova, E.G. Gordeev, V.P. Ananikov, Biological activity of ionic liquids and their application in pharmaceutics and medicine, Chem. Rev. 117 (10) (2017) 7132–7189.
[33] M. Goldfeder, A. Fishman, Modulating enzyme activity using ionic liquids or surfactants, changes in tyrosinase specificity by ionic liquids and sodium dodecyl sulfate, Appl. Microbiol. Biotechnol. 98 (2) (2014) 545–554.
[34] H. Zhao, Protein stabilization and enzyme activation in ionic liquids: specific ion effects, methods for stabilizing and activating enzymes in ionic liquids—a review, J. Chem. Technol. Biotechnol. 91 (1) (2016) 25–50.
[35] Z. Yang, Hofmeister effects: an explanation for the impact of ionic liquids on biocatalysis, J. Biotechnol. 144 (1) (2009) 12–22.
[36] H. Zhao, O. Olubajo, Z. Song, A.L. Sims, T.E. Person, R.A. Lawal, L.A. Holley, Effect of kosmotropicity of ionic liquids on the enzyme stability in aqueous solutions, Bioorg. Chem. 34 (1) (2006) 15–25.
[37] H. Zhao, Are ionic liquids kosmotropic or chaotropic? An evaluation of available thermodynamic parameters for quantifying the ion kosmotropicity of ionic liquids, methods for stabilizing and activating enzymes in ionic liquids—a review, J. Chem. Technol. Biotechnol. 81 (6) (2006) 877–891.
[38] J.-Q. Lai, Z. Li, Y.-H. Lu, Z. Yang, Specific ion effects of ionic liquids on enzyme activity and stability, Green Chem. 13 (7) (2011) 1860–1868.
[39] W.-W. Gao, F.-X. Zhang, G.-X. Zhang, C.-H. Zhou, Key factors affecting the activity and stability of enzymes in ionic liquids and novel applications in biocatalysis, Biochem. Eng. J. 99 (2015) 67–84.
[40] M. Naushad, Z.A. Alothman, A.B. Khan, M. Ali, Effect of ionic liquid on activity, stability, and structure of enzymes: a review, analysis of the driving force that rule the stability of *Lysozyme* in alkylammonium-based ionic liquids, Int. J. Biol. Macromol. 51 (4) (2012) 555–560.
[41] H. Zhao, Effect of ions and other compatible solutes on enzyme activity, and its implication for biocatalysis using ionic liquids, J. Mol. Catal. B Enzym. 37 (1) (2005) 16–25.
[42] M. Goldfeder, M. Egozy, V.S. Ben-Yosef, N. Adir, A. Fishman, Changes in tyrosinase specificity by ionic liquids and sodium dodecyl sulfate, Appl. Microbiol. Biotechnol. 97 (5) (2013) 1953–1961.
[43] DL, A.L. Nelson, Lehninger, M.M. Cox, Lehninger Principles of Biochemistry, W. H. Freeman, 2008.
[44] Spartan'16, Wavefunction Inc., 18401 Von Karman Avenue, Suite 370, Irvine, CA 92612, 2016.
[45] Y. Shao, L.F. Molnar, Y. Jung, J. Kussmann, C. Ochsenfeld, S.T. Brown, A.T.B. Gilbert, L.V. Slipchenko, S.V. Levchenko, D.P. O'Neill, R.A. DiStasio Jr., R.C. Lochan, T. Wang, G.J.O. Beran, N.A. Besley, J.M. Herbert, C. Yeh Lin, T. Van Voorhis, S. Hung Chien, A. Sodt, R.P. Steele, V.A. Rassolov, P.E. Maslen, P.P. Korambath, R.D. Adamson, B. Austin, J. Baker, E.F.C. Byrd, H. Dachsel, R.J. Doerksen, A. Dreuw, B.D. Dunietz, A.D. Dutoi, T.R. Furlani, S.R. Gwaltney, A. Heyden, S. Hirata, C.-P. Hsu, G. Kedziora, R.Z. Khalliulin, P. Klunzinger, A.M. Lee, M.S. Lee, W. Liang, I. Lotan, N. Nair, B. Peters, E.I. Proynov, P.A. Pieniazek, Y. Min Rhee, J. Ritchie, E. Rosta, C. David Sherrill, A.C. Simmonett, J.E. Subotnik, H. Lee Woodcock Iii, W. Zhang, A.T. Bell, A.K. Chakraborty, D.M. Chipman, F.J. Keil, A. Warshel, W.J. Hehre, H.F. Schaefer Iii, J. Kong, A.I. Krylov, P.M.W. Gill, M. Head-Gordon, Advances in methods and algorithms in a modern quantum

chemistry program package, Phys. Chem. Chem. Phys. 8 (27) (2006) 3172–3191.
[46] A.V. Marenich, R.M. Olson, C.P. Kelly, C.J. Cramer, D.G. Truhlar, Self-Consistent reaction field model for aqueous and nonaqueous solutions based on accurate polarized partial charges, J. Chem. Theory Comput. 3 (6) (2007) 2011–2033.
[47] G.M. Morris, R. Huey, W. Lindstrom, M.F. Sanner, R.K. Belew, D.S. Goodsell, A.J. Olson, AutoDock4 and AutoDockTools4: automated docking with selective receptor flexibility, PACKMOL: a package for building initial configurations for molecular dynamics simulations, J. Comput. Chem. 30 (16) (2009) 2785–2791.
[48] O. Trott, A.J. Olson, AutoDock vina: improving the speed and accuracy of docking with a new scoring function, efficient optimization, and multithreading, PACKMOL: a package for building initial configurations for molecular dynamics simulations, J. Comput. Chem. 31 (2) (2010) 455–461.
[49] K.W. Horn, J.W. Rupp, M.P. Heitz, Biocatalytic Activity of Mushroom Tyrosinase in Ionic Liquids: Specific Ion Effects and the Hofmeister Series, 2017.
[50] Y.-F. Lin, Y.-H. Hu, Y.-L. Jia, Z.-C. Li, Y.-J. Guo, Q.-X. Chen, H.-T. Lin, Inhibitory effects of naphthols on the activity of mushroom tyrosinase, analysis of the driving force that rule the stability of *Lysozyme* in alkylammonium-based ionic liquids, Int. J. Biol. Macromol. 51 (1) (2012) 32–36.
[51] A. Grossfield, P. Ren, J.W. Ponder, Ion solvation thermodynamics from simulation with a polarizable force field, J. Am. Chem. Soc. 125 (50) (2003) 15671–15682.
[52] W.-M. Chai, M.-Z. Lin, F.-J. Song, Y.-X. Wang, K.-L. Xu, J.-X. Huang, J.-P. Fu, Y.-Y. Peng, Rifampicin as a novel tyrosinase inhibitor: inhibitory activity and mechanism, analysis of the driving force that rule the stability of *Lysozyme* in alkylammonium-based ionic liquids, Int. J. Biol. Macromol. 102 (2017) 425–430.
[53] Z.-J. Wang, J. Lee, Y.-X. Si, S. Oh, J.-M. Yang, D. Shen, G.-Y. Qian, S.-J. Yin, Toward the inhibitory effect of acetylsalicylic acid on tyrosinase: integrating kinetics studies and computational simulations, Process Biochem. 48 (2) (2013) 260–266.
[54] W.-J. Hu, L. Yan, D. Park, H.O. Jeong, H.Y. Chung, J.-M. Yang, Z.M. Ye, G.-Y. Qian, Kinetic, structural and molecular docking studies on the inhibition of tyrosinase induced by arabinose, analysis of the driving force that rule the stability of *Lysozyme* in alkylammonium-based ionic liquids, Int. J. Biol. Macromol. 50 (3) (2012) 694–700.
[55] L. Gou, Z.-R. Lü, D. Park, S.H. Oh, L. Shi, S.J. Park, J. Bhak, Y.-D. Park, Z.-L. Ren, F. Zou, The effect of histidine residue modification on tyrosinase activity and conformation: inhibition kinetics and computational prediction, J. Biomol. Struct. Dyn. 26 (3) (2008) 395–401.
[56] Z.-R. Lü, L. Shi, J. Wang, D. Park, J. Bhak, J.-M. Yang, Y.-D. Park, H.-W. Zhou, F. Zou, The effect of trifluoroethanol on tyrosinase activity and conformation: inhibition kinetics and computational simulations, Appl. Biochem. Biotechnol. 160 (7) (2010) 1896–1908.
[57] Y.-X. Si, S.-J. Yin, D. Park, H.Y. Chung, L. Yan, Z.-R. Lü, H.-M. Zhou, J.-M. Yang, G.-Y. Qian, Y.-D. Park, Tyrosinase inhibition by isophthalic acid: kinetics and computational simulation, analysis of the driving force that rule the stability of *Lysozyme* in alkylammonium-based ionic liquids, Int. J. Biol. Macromol. 48 (4) (2011) 700–704.
[58] Y.-X. Si, Z.-J. Wang, D. Park, H.Y. Chung, S.-F. Wang, L. Yan, J.-M. Yang, G.-Y. Qian, S.-J. Yin, Y.-D. Park, Effect of hesperetin on tyrosinase: inhibition kinetics integrated computational simulation study, analysis of the driving force that rule the stability of *Lysozyme* in alkylammonium-based ionic liquids, Int. J. Biol. Macromol. 50 (1) (2012) 257–262.
[59] S.-M. Kang, S.-J. Heo, K.-N. Kim, S.-H. Lee, H.-M. Yang, A.-D. Kim, Y.-J. Jeon, Molecular docking studies of a phlorotannin, dieckol isolated from Ecklonia cava with tyrosinase inhibitory activity, Bioorg. Med. Chem. 20 (1) (2012) 311–316.
[60] M. Kumari, J.K. Maurya, M. Tasleem, P. Singh, R. Patel, Probing HSA-Ionic liquid interactions by spectroscopic and molecular docking methods, J. Photochem. Photobiol. B 138 (2014) 27–35.
[61] M. Alijanianzadeh, A.A. Saboury, M.R. Ganjali, H. Hadi-Alijanvand, A.A. Moosavi-Movahedi, The inhibitory effect of ethylenediamine on mushroom tyrosinase, analysis of the driving force that rule the stability of *Lysozyme* in alkylammonium-based ionic liquids, Int. J. Biol. Macromol. 50 (3) (2012) 573–577.
[62] I. Jha, A. Kumar, P. Venkatesu, The overriding roles of concentration and hydrophobic effect on structure and stability of heme protein induced by imidazolium-Based ionic liquids, J. Phys. Chem. B 119 (26) (2015) 8357–8368.
[63] M. Kumari, U.K. Singh, P. Singh, R. Patel, Effect of N-Butyl-N-Methyl-Morpholinium bromide ionic liquid on the conformation stability of human serum albumin, ChemistrySelect 2 (3) (2017) 1241–1249.
[64] M. Kumari, J.K. Maurya, U.K. Singh, A.B. Khan, M. Ali, P. Singh, R. Patel, Spectroscopic and docking studies on the interaction between pyrrolidinium based ionic liquid and bovine serum albumin, Spectrochim. Acta A 124 (2014) 349–356.
[65] M.F. Sanner, A.J. Olson, J.-C. Spehner, Reduced surface: an efficient way to compute molecular surfaces, Biopolymers 38 (3) (1996) 305–320.
[66] L. Lu, Y. Hu, X. Huang, Y. Qu, A bioelectrochemical method for the quantitative description of the hofmeister effect of ionic liquids in aqueous solution, J. Phys. Chem. B 116 (36) (2012) 11075–11080.
[67] D. Constatinescu, C. Herrmann, H. Weingartner, Patterns of protein unfolding and protein aggregation in ionic liquids, Phys. Chem. Chem. Phys. 12 (8) (2010) 1756–1763.

Please cite this article in press as: M.P. Heitz, J.W. Rupp, Int. J. Biol. Macromol. (2017), https://doi.org/10.1016/j.ijbiomac.2017.10.066